Nano Research 2018, 11(3): 1274–1284
https://doi.org/10.1007/s12274-017-1741-x
Research Article
ISSN 1998-0124
CN 11-5974/O4

Lotus root-like porous carbon nanofiber anchored with CoP nanoparticles as all-pH hydrogen evolution electrocatalysts

Hengyi Lu[1], Wei Fan[2] (✉), Yunpeng Huang[1], and Tianxi Liu[1,2] (✉)

[1] *State Key Laboratory of Molecular Engineering of Polymers, Department of Macromolecular Science, Fudan University, 220 Handan Road, Shanghai 200433, China*
[2] *State Key Laboratory for Modification of Chemical Fibers and Polymer Materials, College of Materials Science and Engineering, Donghua University, 2999 North Renmin Road, Shanghai 201620, China*

Received: 11 April 2017
Revised: 7 July 2017
Accepted: 23 July 2017

KEYWORDS
porous carbon nanofiber,
cobalt phosphide,
hydrogen evolution reaction,
all-pH range

ABSTRACT

The development of highly active and cost-effective hydrogen evolution reaction (HER) catalysts is of vital importance to addressing global energy issues. Here, a three-dimensional interconnected porous carbon nanofiber (PCNF) membrane has been developed and utilized as a support for active cobalt phosphide (CoP) nanoparticles. This rationally designed self-supported HER catalyst has a lotus root-like multichannel structure, which provides several intrinsic advantages over conventional CNFs. The longitudinal channels can store the electrolyte and ensure fast ion and mass transport within the catalysts. Additionally, mesopores on the outer and inner carbon walls enhance ion and mass migration of the electrolyte to HER active CoP nanoparticles, thus shortening the ion transport distance and increasing the contact area between the electrolyte and the CoP nanoparticles. Moreover, the conductive carbon substrate provides fast electron transfer pathways by forming an integrated conductive network, which further ensures fast HER kinetics. As a result, the CoP/PCNF composites exhibit low onset-potentials (−20, −91, and −84 mV in 0.5 M H_2SO_4, 1 M PBS, and 1 M KOH, respectively). These findings show that CoP/PCNF composites are promising self-supporting and high-performance all-pH range HER catalysts.

1 Introduction

Hydrogen is recognized as a promising energy carrier due to its carbon-free, environmentally friendly, and renewable nature. In this regard, the electrochemical hydrogen evolution reaction (HER) has emerged as an efficient way to produce H_2. To date, the most effective HER catalyst is platinum (Pt); however, its

Address correspondence to Wei Fan, weifan@dhu.edu.cn; Tianxi Liu, txliu@fudan.edu.cn, txliu@dhu.edu.cn

high price and limited availability prevent its use in large-scale applications [1–3]. The development of high performance, low-cost, and earth abundant HER catalysts capable of replacing Pt is therefore of central to expanding the use of H_2 as an energy carrier.

Over the past several decades, there has been significant progress in the development of high performance HER catalysts. For example, efficient HER has been demonstrated using transition metal chalcogenides [2, 4], nitrides [5], and carbides [6, 7] in acidic electrolytes. Their performance, however, is still far lower than that of Pt in alkaline and neutral environments. This is particularly an issue for water electrolysis systems, which operate in conjunction with the oxygen evolution reaction (alkaline medium) or with microbial electrolysis cells (neutral medium) [8, 9]. The development of Pt-free HER catalysts with high performance in non-acidic environments is therefore of central importance to achieving commercial-scale H_2 production. Recently, transition metal phosphides (TMPs) have attracted much attention as HER catalysts due to their ability to achieve high catalytic activity in a wide pH range [10]. One such example is cobalt phosphide (CoP), which has shown impressive catalytic performance for HER [1, 11–14]. For example, Lewis and Schaal et al. [11] reported that CoP is a highly active and acid-stable HER catalyst, which only requires an applied overpotential of 85 mV to obtain current densities as high as 20 $mA{\cdot}cm^{-2}$ in an acidic electrolyte. However, the use of powder catalysts requires time-consuming preparation of catalyst inks, which have to be deposited on current collectors before use. This decreases the conductivity and is not advisable for practical applications. Additionally, aggregation of nanomaterials is intrinsic to this process and hinders electrocatalytic efficiency by blocking active sites [15].

Hybridizing these electrochemical active nanomaterials with proper self-standing carbon supporting materials is an effective method to overcome these issues [16, 17]. Carbon supporters can not only suppress the aggregation and help the uniform dispersion of active nanoparticles, but also improve the overall conductivity of the hybrid [18]. Specifically, one-dimensional carbon nanofibers (CNFs) with high surface-to-volume ratios are widely used as supports in electrochemical energy-related systems. This is because they improve the accessibility of electrolyte ions and reduce the internal resistance. Furthermore, the self-standing feature of CNF membranes simplifies the electrode fabrication procedure [19]. In this regard, electrospinning is a promising and straightforward technique for the mass production of CNF membranes with good structural stability and high flexibility. Moreover, porous CNFs with tunable porous structures can be easily fabricated by electrospinning, which show great potential in high-performance energy harvesting systems, as they can provide easy access of electrolytes and reduced internal resistance [20].

Inspired by the structure of lotus roots, we have developed a facile and efficient method to construct hierarchical porous carbon nanofibers (PCNF) with lotus root-like longitudinal channels and mesopores. This unique PCNF acts as a support for anchoring electrocatalytically active CoP nanoparticles HER catalysts. Longitudinal channels play a crucial role in storing and transporting oxygen and nutrients for lotus roots. Similar to this, our CoP/PCNF hybrid has longitudinal channels in PCNF, which can act as electrolyte reservoirs, while the mesopores on the carbon walls promote ion and mass migration from the electrolyte to electroactive CoP nanoparticles. This therefore enhances the contact between the electrolyte and CoP nanoparticles. The three-dimensional (3D) interconnected PCNF structure can also form an integrated conductive framework and reduce the electron transfer resistance during the electrochemical reaction process. Moreover, the self-supporting nature of the CoP/PCNF composite membrane can mitigate concerns over the tedious processing methods typical of other electrodes. Consequently, this CoP/PCNF hybrid catalyst exhibits outstanding HER activity in a wide pH range. The onset potential for HER using the CoP/PCNF hybrid is −20 (in 0.5 M H_2SO_4), −91 (in 1 M PBS), and −84 mV (in 1 M KOH) vs. reversible hydrogen electrode (RHE). Remarkably, the CoP/PCNF hybrid requires only an applied overpotential of 83 (acidic electrolyte), 191 (neutral electrolyte), and 138 mV (alkaline electrolyte) to drive a current density of 10 $mA{\cdot}cm^{-2}$. This performance is superior to most

Co-based HER catalysts reported to date.

2 Experimental

2.1 Preparation of PCNF membranes

The spinning solution was prepared by dissolving 0.5 g polyacrylonitrile (PAN) and various amounts of polystyrene (PS) (0.1, 0.3, 0.5 g) in 5 mL N,N-dimethylformamide (DMF) under continuous magnetic stirring at 80 °C for 3 h. PAN/PS nanofibers were first prepared by electrospinning under 20 kV with a feed speed of 1.5 mL·h^{-1}. The distance between the syringe and the aluminum foil collector was fixed at 15 cm. Then, the obtained PAN/PS membranes were heated to 250 °C in air to complete the pre-oxidization process. Finally, the PCNF membranes were obtained by carbonization of the PAN/PS membranes at 800 °C for 2 h under N_2 atmosphere with a heating rate of 5 °C·min^{-1}. Electrospun pure PAN nanofibers were also prepared and further carbonized to obtain carbon nanofibers (CNF).

2.2 Preparation of Co_3O_4/PCNF hybrids

Co_3O_4/PCNF hybrids were synthesized through a simple one-step hydrothermal method. First, the PCNF membranes were treated by 2 M HNO_3 at 40 °C for 6 h to increase their hydrophilicity. Then, 10 mg of treated PCNF membranes were immersed in a 20 mL aqueous solution (20 h). The starting concentrations of $Co(CH_3COO)_2{\cdot}4H_2O$ were varied (0.2, 0.4, 0.6, 0.8 mmol). Next, 4 mL of 25% NH_4OH was slowly added into the above mixture under gentle shaking and allowed to stand for another 10 min before heating under hydrothermal conditions at 180 °C (3 h). The collected black membranes were washed with deionized (DI) water and ethanol three times before drying at 60 °C for 12 h to obtain Co_3O_4/PCNF hybrids.

2.3 Preparation of CoP/PCNF hybrid

The phosphidation process was performed in a tubular furnace, where the NaH_2PO_2 powder was located in the upstream side and the Co_3O_4/PCNF hybrid was placed next to the NaH_2PO_2 at the downstream side. The mass ratio was 1:10 (Co_3O_4/PCNF:NaH_2PO_2) and the furnace was then heated to 350 °C at a ramp rate of 2 °C·min^{-1} and kept for 2 h. After the phosphidation, the composite membranes were immersed in a 0.5 M H_2SO_4 solution for 30 min to remove the residual Co_3O_4 before further washing with DI water and ethanol. The products were named as CoP/PCNF-0.2, CoP/PCNF-0.4, CoP/PCNF-0.6, and CoP/PCNF-0.8, corresponding to the different concentrations of $Co(CH_3COO)_2{\cdot}4H_2O$ (0.2, 0.4, 0.6, 0.8 mmol). Pure CoP and CoP/CNF-0.4 composites were also synthesized via the same procedure both with and without the addition of CNF membranes.

2.4 Characterization

Transmission electron microscopy (TEM), high-resolution TEM (HETEM), scanning transmission electron microscopy (STEM), selected-area electron diffraction (SAED), and energy dispersive X-ray (EDX) observations were conducted on a Tecnai G2 F20 S-Twin TEM instrument under an accelerating voltage of 200 kV. Field emission scanning electron microscopy (FESEM) was performed by a Zeiss Ultra 55 FESEM instrument at an accelerating voltage of 5 kV. X-ray diffraction (XRD) measurements were carried out using a PANalytical X'pert PRO XRD with Cu Kα radiation (operating voltage, 40 kV; cathode current, 40 mA; λ = 0.1542 nm; scan rate, 5 °C·min^{-1}). X-ray photoelectron spectroscopy (XPS) spectra were collected by a VG ESCALAB 220I-XL device. The specific surface area and pore size distribution of PCNF and CoP/PCNF were characterized with a belsorp-max surface area-detecting instrument (Tristar3000) via N_2 physisorption at 77 K. Thermo-gravimetric analysis (TGA, Mettler Toledo TGA1) was carried out with a heating rate of 10 °C·min^{-1} from 100 to 800 °C in air. Gas chromatography (GC) measurements were conducted on a GC2060 instrument (Shanghai Ramiin Instruments, China).

2.5 Electrochemical characterization

Electrochemical measurements were carried out in a conventional three-electrode cell on a CHI 660D electrochemical workstation (Shanghai Chenhua Instruments, China) with a graphite rod as the counter electrode and a saturated calomel electrode (SCE) as the reference electrode. To prepare the working

electrode, a piece of CoP/PCNF membrane (~ 3 mm × 3 mm) was attached to the glassy carbon electrode by Nafion (5 wt.%) and left to dry at room temperature. The linear sweep voltammetry (LSV) measurements were carried out in N_2 saturated 0.1 M KOH, 1 M PBS, and 1 M KOH solutions, respectively. The scan rate used to evaluate the HER performance was 2 mV·s^{-1}. To calculate the double-layer capacitance (C_{dl}) of CoP/CNF and CoP/PCNF, cyclic voltammetry (CV) measurements were carried at different scan rates in 0.5 M H_2SO_4. By plotting the Δj at 0.2 V vs. RHE against the scan rate, the slope is twice that of C_{dl}. Electrochemical impedance spectroscopic (EIS) measurements were carried out under various overpotentials in the frequencies ranging from 106 to 10^{-2} Hz with an amplitude of 5 mV. All the potentials were calibrated to the RHE according to the equation of $E_{RHE} = E_{SCE} + (0.241 + 0.059\ pH)$ V.

3 Results and discussion

The typical preparation procedure for a CoP/PCNF composite is shown in Scheme 1. To obtain the PCNF membranes, a mixed solution of PAN and PS was electrospun into nanofibrous membranes through a single-nozzle electrospinning technique. Due to poor compatibility between PAN and PS, they will exist as separate phases in DMF [21–23]. During the electrospinning process, along with the finning and drawing process of the continuous phase (PAN), the PS phase was drastically stretched along the longitudinal direction within the PAN fibers. Next, we thermally decomposed PS to form channels and pores. PAN was converted into carbon during the calcination process resulting in a lotus-root like structure [21]. We then characterized the microstructure of PCNF using SEM (Figs. 1(a) and 1(b)). Nano-channels (~ 20 to 60 nm in diameter) are generated from the decomposition of PS. These channels are capable of increasing the absorbability and facilitating transport of the electrolyte. The porosity of PCNF is controlled by adjusting the starting concentration of PS (Fig. S1 in the Electronic Supplementary Material (ESM)). Clearly, increasing the PS content increases the porosity, pore size, and the diameter of PCNF. It is also worth noting that further increase in PS content eventually generates mesopores on the surface and carbon walls on the interior of PCNF (PAN/PS = 0.5/0.3 in Fig. 1(b) and 0.5/0.5 in Fig. S1(d) in the ESM). Mesopores improve the contact between the electrolyte and the active materials anchored on PCNF, thus generating more active sites for electrochemical reactions. However, if the PS content is too high, the formability and flexibility of the PCNF membrane will eventually decrease (e.g., PAN/PS ratio of 0.5/0.5). Furthermore, the increasing diameter of nanofibers with increased PS content decreases the active material loading. Taking the above factors into consideration, the optimal PAN/PS mass ratio was determined to be 0.5/0.3. All subsequent experiments use membranes fabricated with this PAN/PS mass ratio.

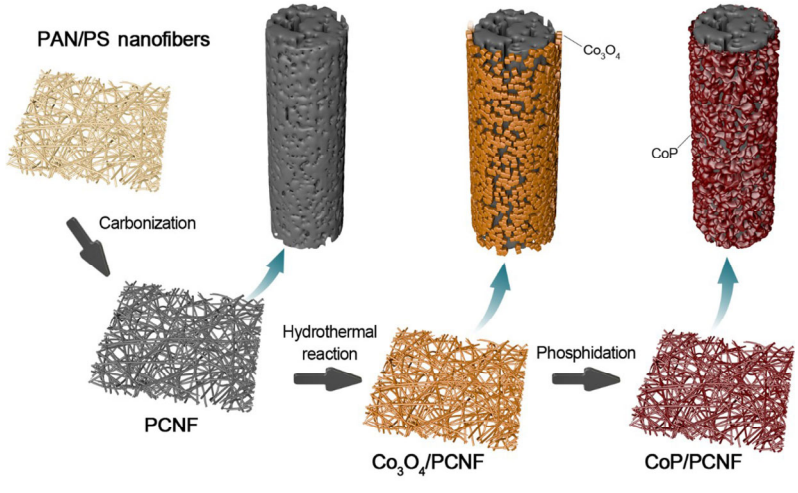

Scheme 1 The preparation of the CoP/PCNF hybrids.

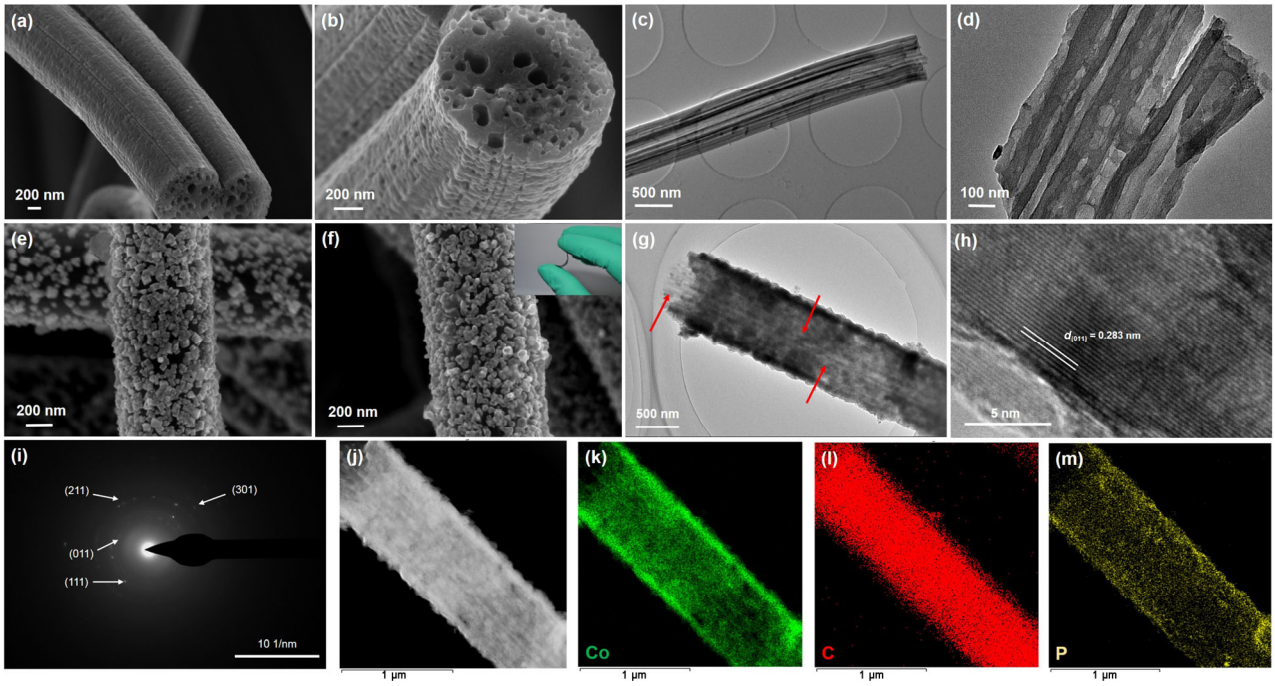

Figure 1 ((a) and (b)) SEM and ((c) and (d)) TEM images of PCNF (PAN/PS = 0.5/0.3). (e) SEM image of Co_3O_4/PCNF. (f) SEM image of CoP/PCNF. ((g) and (h)) TEM images of CoP/PCNF. (i) SAED pattern of CoP nanoparticle. ((j)–(m)) STEM image and EDX elemental mappings of Co, C, and P of CoP/PCNF.

The TEM images of PCNF directly show unbroken individual fibers with parallel porous structures (Fig. 1(c)), which can interconnect to form a conductive 3D network with hierarchical porous structures. High-resolution TEM images (Fig. 1(d)) further reveal a large concentration of mesopores existing both on the surface and on the inner carbon walls of PCNF. This unique mesoporous structure allows the electrolyte to fill the PCNF channels, resulting in an enlarged contact area and enhanced electron and mass transport between the catalyst and the electrolyte.

We then used a two-step method to prepare CoP/PCNF composites. First, Co_3O_4/PCNF composites were prepared using a simple hydrothermal method in accordance with our previous work [24]. Figure 1(e) shows Co_3O_4 nanocubes (~ 20 to 50 nm) uniformly anchored on the surface of PCNF. Aggregation appears to be negligible. After gas phosphidation at a low temperature, the Co_3O_4 nanocubes are converted into irregularly shaped CoP nanoparticles. However, the average size and uniform distribution are well retained (Fig. 1(f)). This indicates that the contact between CoP nanoparticles and PCNF is intimate. The CoP/PCNF composite membrane are self-supported (inset of Fig. 1(f)). The TEM images of the CoP/PCNF sample also show that thin layers of CoP nanoparticles are uniformly coated on PCNF. The channels in PCNF are well preserved after a series of chemical treatments as indicated by the red arrows in Fig. 1(g). HRTEM image in Fig. 1(h) clearly shows the lattice fringes with an interplane distance of 0.283 nm corresponding to the (011) plane of the CoP nanoparticles, which confirms that the crystalline structure is unaltered. The SAED pattern (Fig. 1(i)) exhibits several well-defined rings, which can be assigned to the (011), (111), (211), and (301) facets of orthorhombic CoP. Additionally, STEM image (Fig. 1(j)) and EDX elemental maps (Figs. 1(k)–1(m)) were also collected to reveal the distribution of Co, C, and P elements in CoP/PCNF.

We optimize the HER performance by altering the CoP content in the composite. We do this through the phosphidation of Co_3O_4/PCNF precursors with different starting ratios. SEM images for Co_3O_4/PCNF composites with different mass loading are shown in Fig. S2 in the ESM. The Co_3O_4 nanocubes are well dispersed with PCNF for all samples. The density and size of Co_3O_4 nanocubes increases with increasing Co_3O_4

content (Fig. S3 in the ESM). For the CoP/PCNF-0.2 sample, the surface of PCNF is readily apparent, thus indicating a sparse distribution of CoP nanoparticles within PCNF. As shown in Figs. S3(c) and S3(d) in the ESM, the CoP nanoparticles have a more uniform size distribution in the CoP/PCNF-0.4 composite, which also achieves complete surface coverage of PCNF. TGA experiments show that CoP/PCNF-0.4 has a CoP content of 69 wt.% (Fig. S4 in the ESM). The relatively small size and uniform distribution of CoP nanoparticles in our nanostructures may effectively enhance the activity of the electroactive sites in HER processes. If, on the other hand, the starting concentration of the cobalt salt is too high (e.g., CoP/PCNF-0.6 and CoP/PCNF-0.8 hybrids), the CoP nanoparticles become dense, which inevitably leads to accumulation and the formation of large aggregates (Figs. S3(e)–S3(h) in the ESM). This eventually impedes performance by raising the contact resistance between the electrolyte and active nanoparticles. Conversely, pure CoP nanoparticles fabricated by the same process tend to aggregate into large clusters, which greatly hinders the exposure of the electroactive sites in CoP (Fig. S5 in the ESM).

XRD studies further confirm the successful transformation of Co_3O_4/PCNF to CoP/PCNF (Fig. 2(a)). A broad peak centered at $2\theta = 26.4°$ for PCNF is attributed to the amorphous carbon derived from the carbonized PAN; all other peaks are consistent with the standard patterns for Co_3O_4 and CoP, respectively [25, 26]. XPS is used to analyze the surface elemental composition and the chemical states of the CoP/PCNF-0.4 sample (Figs. 2(b)–2(d)). The spectrum confirms the coexistence of C, Co, O, and P elements within the composite without any detectable impurities. Figure 2(c) shows that the peak of Co 2p can be deconvoluted into two peaks of Co $2p_{3/2}$ and Co $2p_{1/2}$, respectively. The Co $2p_{3/2}$ region shows two main peaks at 779.0 and 782.0 eV with one satellite peak at 786.2 eV. The Co $2p_{1/2}$ region exhibits two main peaks at 793.9 and 798.2 eV with a satellite peak at 803.3 eV. The high-resolution P 2p region (Fig. 2(d)) shows three peaks at 129.1, 129.9, and 132.8 eV corresponding to the P $2p_{3/2}$ and P $2p_{1/2}$ states in the CoP nanocrystals and oxidized P species, respectively [27–29]. The binding energy of Co 2p is shifted in a positive direction (779.0 eV vs. 778.1 eV) in comparison with that of metallic Co. Conversely, the P 2p peak shifts in a negative direction with respect to that of elemental P (129.1 eV vs. 130.2 eV). These results suggest that cobalt has a partial positive charge, while phosphorus has

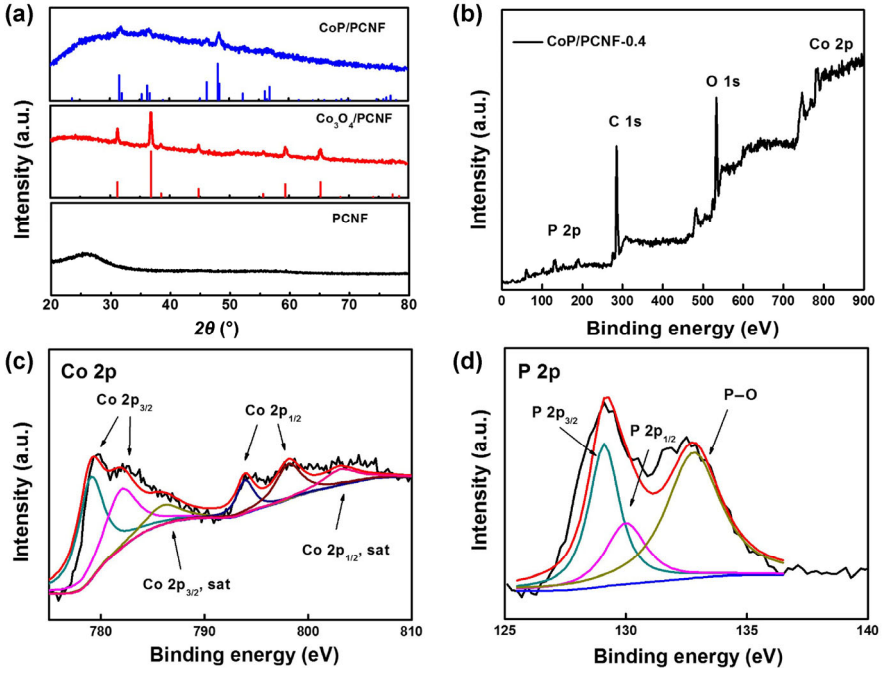

Figure 2 (a) XRD patterns of PCNF, Co_3O_4/PCNF-0.4 and CoP/PCNF-0.4 samples, (b) XPS survey spectrum of CoP/PCNF-0.4, (c) high resolution Co 2p spectrum, and (d) high resolution P 2p spectrum.

a partial negative charge. Hence, electron density is transferred from Co to P, and it would promote adsorption and desorption of reactant and products molecules, respectively. The P centers could promote the formation of cobalt hydride, which could facilitate the following H_2 evolution by electrochemical desorption [1, 17, 18, 29, 30].

To investigate the electrochemical performance of the CoP/PCNF composites, we perform LSV measurements in 0.5 M H_2SO_4 at a scan rate of 2 mV·s^{-1} (Fig. 3(a)). As expected, Pt exhibits excellent HER activity with a near zero onset-potential. All the CoP/PCNF composites show better HER performance than pure CoP. This is because the high conductivity of PCNF provides fast electron transfer pathways during the HER process, as inferred from the Nyquist plots of CoP and CoP/PCNF (Fig. 3(b)). Among the CoP/PCNF composites, optimal performance is achieved with CoP/PCNF-0.4, which exhibits an onset-potential of −20 mV vs. RHE. Furthermore, CoP/PCNF-0.4 delivers a current density (j) of 10.0 mA·cm^{-2} at the low overpotential (η) of 83 mV. Additionally, we observe a rapid increase in current at negative potentials, thus suggesting CoP/PCNF-0.4 can act as a highly active catalyst for hydrogen generation from water in acidic media. The other three LSV curves have negative shifts compared with that of CoP/PCNF-0.4, thus implying inferior HER performance. Morphological changes during the electrochemical process may provide a possible explanation for the different electrocatalytic activities. In comparison to the other three composites, CoP/PCNF-0.4 has an optimal hierarchical structure. The uniformly distributed small CoP nanoparticles, which do not aggregate, result in a large contact area between the electrolyte and catalyst. This, in turn, improves HER performance by facilitating ion/electron transfer. The HER performance of powder (p-CoP/PCNF-0.4) was also studied. The performance was inferior to the CoP/PCNF-0.4 membrane. This can be explained by the formation of short, individual fibers of PCNF, which impedes their ability to form an interconnected 3D conductive network. These results further confirm that the integrated conductive framework is beneficial for the HER process. The Tafel slope of CoP/PCNF-0.4 hybrid is ~ 62 mV·dec^{-1} as shown in Fig. 3(c), therefore

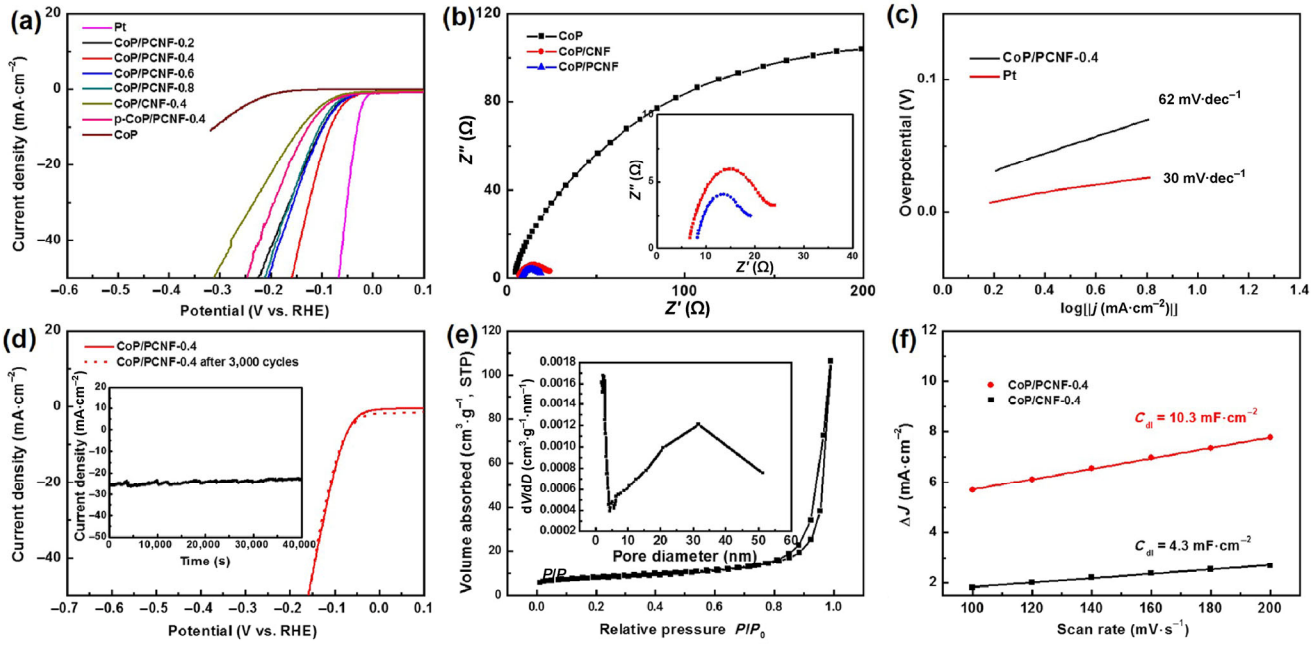

Figure 3 (a) LSV curves of CoP/PCNF hybrids with different CoP contents, CoP/CNF-0.4, p-CoP/PCNF-0.4, pure CoP, and Pt-C in 0.5 M H_2SO_4. (b) Nyquist plots of CoP, CoP/PCNF-0.4, and CoP/CNF-0.4 at −0.22 V vs. RHE. (c) Tafel plots of Pt and CoP/PCNF-0.4. (d) Chronoamperometry i–t curves (inset), LSV curves of CoP/PCNF before and after cycling in 0.5 M H_2SO_4. (e) The nitrogen adsorption/desorption isotherms and BJH pore size distribution (inset) of PCNF. (f) Plots showing the extraction of the double layer capacitance (C_{dl}) for CoP/CNF-0.4 and CoP/PCNF-0.4 hybrids at 0.2 V.

indicating that the HER proceeds through a Volmer–Heyrovsky mechanism. This occurs via the rapid discharge Volmer reaction followed by a rate limiting electrochemical desorption Heyrovsky reaction [10]. The LSV curves (Fig. 3(d)) for CoP/PCNF-0.4 are relatively unaltered after 3,000 cyclic voltammetry cycles. As shown by *i*–*t* curves (inset in Fig. 3(d)), CoP/PCNF-0.4 is able to maintain its high current density continuously for 40,000 s. These results indicate that CoP/PCNF exhibits a superior long-term stability in 0.5 M H_2SO_4.

The electrocatalytic performance of a CoP/CNF composite (CoP/CNF-0.4) is also investigated. As shown in Fig. 3(a), CoP/PCNF-0.4 has a much smaller onset-potential and larger current density than CoP/CNF, thus suggesting that CoP/PCNF is a better catalyst. Additionally, the semicircles of the Nyquist plots in Fig. 3(b) show a much smaller charge-transfer resistance (R_{ct}) for CoP/PCNF in comparison with CoP/CNF. This also suggests that electron transfer is more efficient for the CoP/PCNF catalyst. The higher activity of CoP/PCNF might be due to the porous structure, which can increase the contact area between the catalyst and electrolyte. In order to confirm this line of reasoning, we measured the specific surface areas of PCNF and CoP/PCNF. The nitrogen adsorption/desorption isotherms (Fig. 3(e)) reveal that the specific surface area of PCNF is 39.8 $m^2 \cdot g^{-1}$, which is much larger than that of conventional CNF (usually below 5 $m^2 \cdot g^{-1}$) [31]. The pore size distribution indicates that PCNF has well developed micropores (< 2 nm) and mesopores (2–50 nm), which is consistent with the TEM results. The specific surface area of CoP/PCNF-0.4 (27.2 $m^2 \cdot g^{-1}$) (Fig. S6 in the ESM) is somewhat smaller than that of PCNF and the pore size distribution reveals that the large distribution of micropores/mesopores are well retained in the CoP/PCNF composites. This ensures sufficient contact between the catalyst and electrolyte. The double-layer capacitance (C_{dl}) is another parameter that is affected by the interfacial contact between the surface of the electrode and electrolyte [32]. CV curves at different scan rates show that the C_{dl} value for CoP/PCNF is more than twice that of CoP/CNF (Fig. 3(f) and Fig. S7 in the ESM). This serves as further evidence of the catalytic superiority of PCNF.

The structural origin of the better electrocatalytic performance of CoP/PCNF is described in Scheme 2. Similar to the storage and transport of oxygen and nutrients in lotus-root channels, the longitudinal channels in PCNF (diameters ~ 20 to 60 nm) can serve as electrolyte reservoirs to ensure fast ion transport within the catalyst. The electrolyte fills all of the PCNF channels, thus facilitating the migration of electrolyte ions inside the channels and through the mesopores before reaching the CoP nanoparticles. This greatly decreases the ion transport distance and increases the number of active sites. Comparatively, this effect is not present in the CoP/CNF composite, thus resulting in a smaller contact surface area. Therefore, the CoP/PCNF composites exhibit higher electrochemical activity than CoP/CNF.

We then measured the Faradic efficiency (FE) of CoP/PCNF-0.4. Potentiostatic electrolysis of CoP/PCNF was performed and maintained 60 min at an overpotential of 150 mV in 0.5 M H_2SO_4. Involved gases were measured by GC and only H_2 was detected. The amount of generated H_2 can also be obtained from GC. The amount of experimentally quantified hydrogen agrees well with theoretically calculated hydrogen (assuming 100% FE), suggesting the FE is close to 100%, as shown in Fig. 4).

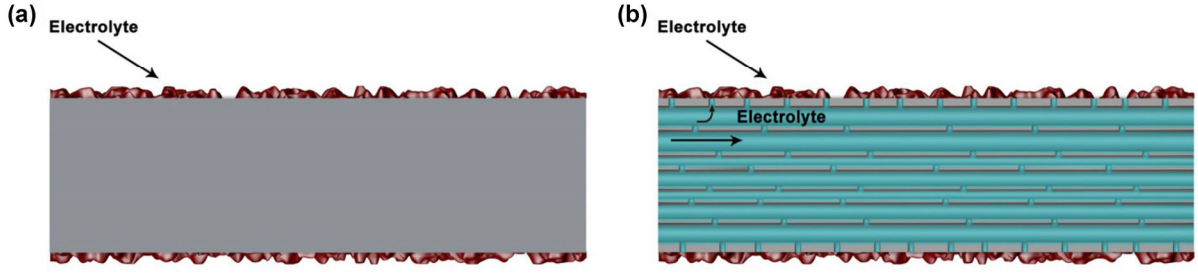

Scheme 2 Schematic illustration showing the contacts between (a) CoP/CNF or (b) CoP/PCNF hybrids and the electrolyte.

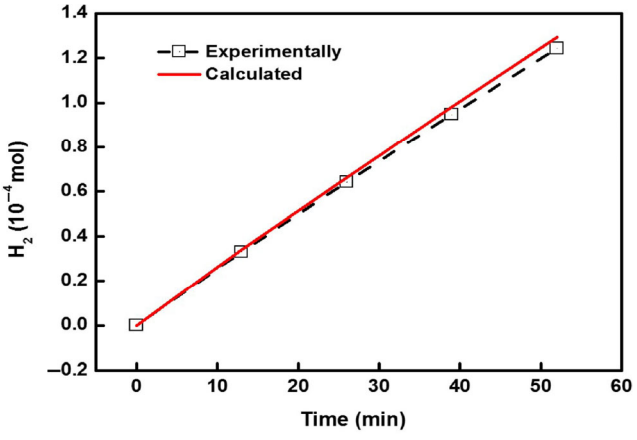

Figure 4 The theoretically calculated and experimentally measured amount of evolved hydrogen versus time for CoP/PCNF-0.4 composite at an overpotential of 150 mV in 0.5 M H_2SO_4.

The HER performance of CoP/PCNF is further evaluated in 1.0 M KOH and 1.0 M PBS solution to determine its applicability as an all-pH-range electrocatalyst (Fig. 5). Notably, the CoP/PCNF electrode also works efficiently in an alkaline (1 M KOH) electrolyte (Figs. 5(a)–5(c)). The low onset-potential (−84 mV vs. RHE) and Tafel slope (81 mV·dec^{-1}) show that the catalyst exhibits fast HER kinetics. Further, a low overpotential of 138 mV can exhibit current densities as high as 10 mA·cm^{-2}, which surpasses the performance of most non-noble metal catalysts reported in the literature. Comparatively, the onset potential for the same process in neutral conditions (Figs. 5(d)–5(f)) is −91 mV (vs. RHE), while the overpotential needed to reach a current density of 10 mA·cm^{-2} is 191 mV. The inferior performance in 1 M PBS is due to the inherently slow kinetics of the HER process in a neutral electrolyte. However, its performance is still competitive with other reported catalysts [2, 6]. Table S1 (in the ESM) summarizes the HER activities of some TMP-based catalysts obtained from recent literature. CoP/PCNF performed well when compared with these catalysts. LSV curves after 3,000 CV cycles and *i*–*t* curves in 1 M KOH (Figs. 5(a) and 5(b)) show a slight activity decay. A possible explanation for this phenomenon is that the strongly corrosive KOH erodes the carbon carriers during the reaction process, thus resulting in the detachment of CoP nanoparticles. CoP/PCNF exhibits superior long-term stability in neutral electrolytes (Fig. 5(e)). SEM images (Fig. S8 in the ESM) after cycling do not show any obvious structural changes, therefore indicating that CoP/PCNF is structurally stable during the hydrogen evolution reaction. These results, together, show that CoP/PCNF has outstanding electrocatalytic activity, a high anti-corrosion stability over a wide pH range, and is therefore a promising catalyst for HER.

4 Conclusions

In summary, PCNF with a lotus-root like multichannel structure was developed and utilized as a supporting template for anchoring HER active CoP nanoparticles.

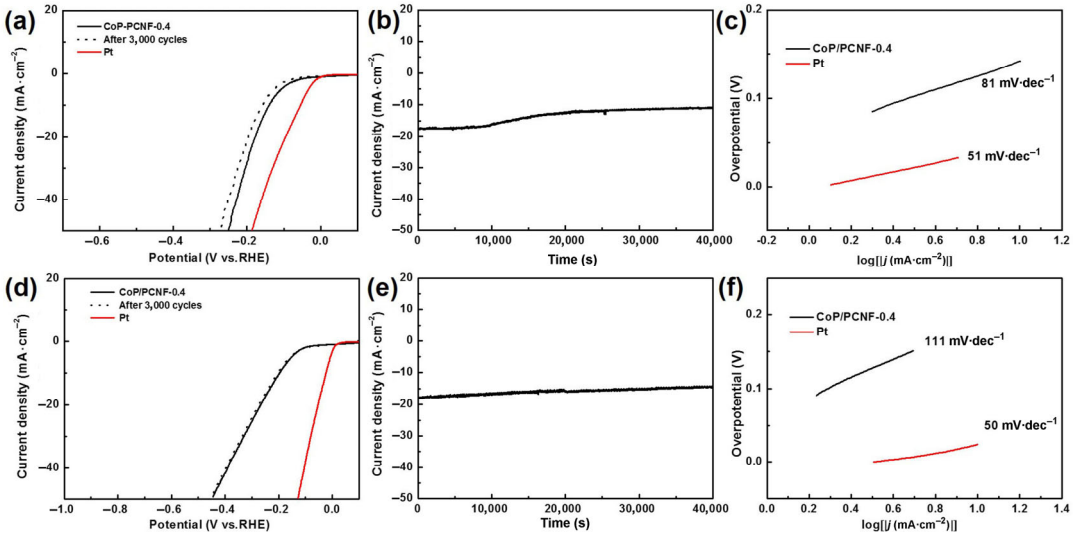

Figure 5 (a) LSV curves, (b) chronoamperometry *i*–*t* curves and (c) Tafel plots of CoP/PCNF and Pt in 1 M KOH. (d) LSV curves, (e) chronoamperometry *i*–*t* curves, and (f) Tafel plots of CoP/PCNF and Pt in 1 M PBS.

These self-supporting CoP/PCNF composite membranes have unique longitudinal channels integrated with mesopores on the outer and inner carbon walls. This, in turn, efficiently improves the contact between CoP and the electrolyte, thus increasing the number of HER active sites. Moreover, the conductive carbon substrate forms an interconnected conductive network, providing fast electron transfer pathways, which further ensures fast HER kinetics. When being directly used as HER catalyst within a wide pH range, the CoP/PCNF hybrid membranes exhibit performances competitive with other non-noble metal HER catalysts. Furthermore, this highly conductive flexible porous carbon nanofiber membrane may be easily extended to other electrochemical energy systems such as lithium ion batteries, Li-S batteries, and supercapacitors.

Acknowledgements

The authors are grateful for the financial support from the National Natural Science Foundation of China (Nos. 51433001 and 51373037), the Program of Shanghai Academic Research Leader (No. 17XD1400100).

Electronic Supplementary Material: Supplementary material (SEM images of PCNF samples, Co_3O_4/PCNF samples, CoP/PCNF samples, pure Co_3O_4, pure CoP, CoP/PCNF after HER tests; TGA curves, characterization of porous properties, CV curves of CoP/PCNF, CV curves of CoP/CNF; performance comparisons) is available in the online version of this article at https://doi.org/10.1007/s12274-017-1741-x.

References

[1] Zou, X. X.; Zhang, Y. Noble metal-free hydrogen evolution catalysts for water splitting. *Chem. Soc. Rev.* **2015**, *44*, 5148–5180.

[2] Voiry, D.; Yang, J.; Chhowalla, M. Recent strategies for improving the catalytic activity of 2D TMD nanosheets toward the hydrogen evolution reaction. *Adv. Mater.* **2016**, *28*, 6197–6206.

[3] Jiao, Y.; Zheng, Y.; Jaroniec, M.; Qiao, S. Z. Design of electrocatalysts for oxygen- and hydrogen-involving energy conversion reactions. *Chem. Soc. Rev.* **2015**, *44*, 2060–2086.

[4] Chang, Y. H.; Wu, F. Y.; Chen, T. Y.; Hsu, C. L.; Chen, C. H.; Wiryo, F.; Wei, K. H.; Chiang, C. Y.; Li, L. J. Three-dimensional molybdenum sulfide sponges for electrocatalytic water splitting. *Small* **2014**, *10*, 895–900.

[5] Xie, J. F.; Li, S.; Zhang, X. D.; Zhang, J. J.; Wang, R. X.; Zhang, H.; Pan, B. C.; Xie, Y. Atomically-thin molybdenum nitride nanosheets with exposed active surface sites for efficient hydrogen evolution. *Chem. Sci.* **2014**, *5*, 4615–4620.

[6] Wan, C.; Leonard, B. M. Iron-doped molybdenum carbide catalyst with high activity and stability for the hydrogen evolution reaction. *Chem. Mater.* **2015**, *27*, 4281–4288.

[7] Ang, H.; Wang, H. W.; Li, B.; Zong, Y.; Wang, X. F.; Yan, Q. Y. 3D hierarchical porous Mo_2C for efficient hydrogen evolution. *Small* **2016**, *12*, 2859–2865.

[8] Subbaraman, R.; Tripkovic, D.; Strmcnik, D.; Chang, K. C.; Uchimura, M.; Paulikas, A. P.; Stamenkovic, V.; Markovic, N. M. Enhancing hydrogen evolution activity in water splitting by tailoring Li^+-$Ni(OH)_2$-Pt interfaces. *Science* **2011**, *334*, 1256–1260.

[9] Kundu, A.; Sahu, J. N.; Redzwan, G.; Hashim, M. A. An overview of cathode material and catalysts suitable for generating hydrogen in microbial electrolysis cell. *Int. J. Hydrogen Energy* **2013**, *38*, 1745–1757.

[10] Xiao, P.; Chen, W.; Wang, X. A review of phosphide-based materials for electrocatalytic hydrogen evolution. *Adv. Energy Mater.* **2015**, *5*, 1500985.

[11] Popczun, E. J.; Read, C. G.; Roske, C. W.; Lewis, N. S.; Schaak, R. E. Highly active electrocatalysis of the hydrogen evolution reaction by cobalt phosphide nanoparticles. *Angew. Chem., Int. Ed.* **2014**, *126*, 5531–5534.

[12] Huang, Z. P.; Chen, Z. Z.; Chen, Z. B.; Lv, C. C.; Humphrey, M. G.; Zhang, C. Cobalt phosphide nanorods as an efficient electrocatalyst for the hydrogen evolution reaction. *Nano Energy* **2014**, *9*, 373–382.

[13] Jiang, P.; Liu, Q.; Ge, C. J.; Cui, W.; Pu, Z. H.; Asiri, A. M.; Sun, X. P. CoP nanostructures with different morphologies: Synthesis, characterization and a study of their electrocatalytic performance toward the hydrogen evolution reaction. *J. Mater. Chem. A* **2014**, *2*, 14634–14640.

[14] Yang, J.; Zhang, Y.; Sun, C. C.; Liu, H. Z.; Li, L. Q.; Si, W. L.; Huang, W.; Yan, Q. Y.; Dong, X. C. Graphene and cobalt phosphide nanowire composite as an anode material for high performance lithium-ion batteries. *Nano Res.* **2016**, *9*, 612–621.

[15] Liao, L.; Zhu, J.; Bian, X. J.; Zhu, L. N.; Scanlon, M. D.; Girault, H. H.; Liu, B. H. MoS_2 formed on mesoporous graphene as a highly active catalyst for hydrogen evolution. *Adv. Funct. Mater.* **2013**, *23*, 5326–5333.

[16] Huang, H. J.; Wang, X. Recent progress on carbon-based support materials for electrocatalysts of direct methanol fuel cells. *J. Mater. Chem. A* **2014**, *2*, 6266–6291.

[17] Li, M.; Liu, X. T.; Xiong, Y. P.; Bo, X. J.; Zhang, Y. F.; Han, C.; Guo, L. P. Facile synthesis of various highly dispersive CoP nanocrystal embedded carbon matrices as efficient electrocatalysts for the hydrogen evolution reaction. *J. Mater. Chem. A* **2015**, *3*, 4255–4265.

[18] Liu, Q.; Tian, J. Q.; Cui, W.; Jiang, P.; Cheng, N. Y.; Asiri, A. M.; Sun, X. P. Carbon nanotubes decorated with CoP nanocrystals: A highly active non-noble-metal nanohybrid electrocatalyst for hydrogen evolution. *Angew. Chem., Int. Ed.* **2014**, *53*, 6710–6714.

[19] Zhang, B.; Kang, F. Y.; Tarascon, J. M.; Kim, J. K. Recent advances in electrospun carbon nanofibers and their application in electrochemical energy storage. *Prog. Mater. Sci.* **2016**, *76*, 319–380.

[20] He, H. Y.; Shi, L.; Fang, Y.; Li, X. L.; Song, Q.; Zhi, L. J. Mass production of multi-channeled porous carbon nanofibers and their application as binder-free electrodes for high-performance supercapacitors. *Small* **2014**, *10*, 4671–4676.

[21] Li, Z.; Zhang, J. T.; Chen, Y. M.; Li, J.; Lou, X. W. D. Pie-like electrode design for high-energy density lithium-sulfur batteries. *Nat. Commun.* **2015**, *6*, 8850.

[22] Zhou, Q. H.; Li, Z. Y.; Liang, H. Q.; Long, Y. J.; Wu, Q.; Gao, H. Y.; Liang, G. D.; Zhu, F. M. Crystallization-driven self-assembly of isotactic polystyrene in *N, N*-dimethylformamide. *Chin. J. Polym. Sci.* **2015**, *33*, 646–651.

[23] Marwat, Z. K.; Baloch, M. K. Miscibility between PS and PSAN affected by solvent and temperature of the system. *Chin. J. Polym. Sci.* **2014**, *32*, 1442–1449.

[24] Lu, H. Y.; Huang, Y. P.; Yan, J. J.; Fan, W.; Liu, T. X. Nitrogen-doped graphene/carbon nanotube/Co_3O_4 hybrids: One-step synthesis and superior electrocatalytic activity for the oxygen reduction reaction. *RSC Adv.* **2015**, *5*, 94615–94622.

[25] Xu, C. H.; Sun, J.; Gao, L. A. Controllable synthesis of triangle taper-like cobalt hydroxide and cobalt oxide. *CrystEngComm.* **2011**, *13*, 1586–1590.

[26] Infantes-Molina, A.; Cecilia, J. A.; Pawelec, B.; Fierro, J. L. G.; Rodríguez-Castellón, E.; Jiménez-López, A. Ni_2P and CoP catalysts prepared from phosphite-type precursors for HDS–HDN competitive reactions. *Appl. Catal. A* **2010**, *390*, 253–263.

[27] Yang, F. L.; Chen, Y. T.; Cheng, G. Z.; Chen, S. L.; Luo, W. Ultrathin nitrogen-doped carbon coated with CoP for efficient hydrogen evolution. *ACS Catal.* **2017**, *7*, 3824–3831.

[28] Liu, M. J.; Li, J. H. Cobalt phosphide hollow polyhedron as efficient bifunctional electrocatalysts for the evolution reaction of hydrogen and oxygen. *ACS Appl. Mater. Interfaces* **2016**, *8*, 2158–2165.

[29] Pan, Y.; Lin, Y.; Chen, Y. J.; Liu, Y. Q.; Liu, C. G. Cobalt phosphide-based electrocatalysts: Synthesis and phase catalytic activity comparison for hydrogen evolution. *J. Mater. Chem. A* **2016**, *4*, 4745–4754.

[30] Tian, J. Q.; Liu, Q.; Asiri, A. M.; Sun, X. P. Self-supported nanoporous cobalt phosphide nanowire arrays: An efficient 3D hydrogen-evolving cathode over the wide range of pH 0–14. *J. Am. Chem. Soc.* **2014**, *136*, 7587–7590.

[31] Miao, Y. E.; Huang, Y. P.; Zhang, L. S.; Fan, W.; Lai, F. L.; Liu, T. X. Electrospun porous carbon nanofiber@MoS_2 core/sheath fiber membranes as highly flexible and binder-free anodes for lithium-ion batteries. *Nanoscale* **2015**, *7*, 11093–11101.

[32] Xu, K.; Wang, F. M.; Wang, Z. X.; Zhan, X. Y.; Wang, Q. S.; Cheng, Z. Z.; Safdar, M.; He, J. Component-controllable $WS_{2(1-x)}Se_{2x}$ nanotubes for efficient hydrogen evolution reaction. *ACS Nano* **2014**, *8*, 8468–8476.